BCC-Splines: Generalization of B-Splines for the Body-Centered Cubic Lattice

Balázs Csébfalvi
Department of Control Engineering and Information Technology
Budapest University of Technology and Economics
Magyar tudósok krt. 2, Budapest, Hungary, H-1117
E-mail: cseb@iit.bme.hu

ABSTRACT

Recently, the B-spline family of reconstruction filters has been generalized for the hexagonal lattice, which is optimal for sampling 2D circularly band-limited signals. In this paper, we extend this generalization to the body-centered cubic (BCC) lattice, which is optimal for sampling spherically band-limited 3D signals. We call the obtained new reconstruction filters BCC-splines. Although the explicit analytical formulas are not defined yet, we evaluate the discrete approximation of these filters in the frequency domain in order to analyze their performance in a volume-rendering application. Our experimental results show that the BCC-splines can be superior over the box splines previously proposed for the BCC lattice.

Keywords: Optimal Regular Volume Sampling, Body-Centered Cubic Lattice, Reconstruction, Volume Rendering.

1 INTRODUCTION

Volumetric data usually contains the samples of a continuous signal sampled on a Cartesian lattice. This representation is still the most popular one in practice, as it has obvious advantageous properties. For example, the samples are easy to store in a 3D array, and a continuous reconstruction can be efficiently implemented by a fast separable convolution. However, it is well-known that the Cartesian lattice is not optimal for sampling spherically band-limited 3D signals [TMG01], even if the sampling distance is the same along the three major axes yielding a Cartesian cubic (CC) lattice. Although the shape of the spectrum is usually not known in advance, it is not favorable if the sampling scheme prefers specific directions in the frequency domain [EM06]. Therefore, the assumption that the spectrum of the original signal is bounded by a sphere seems to be natural.

When a signal is sampled on a specific lattice, the original primary spectrum gets replicated around the points of the dual or reciprocal lattice [OS89], which is the Fourier transform of the sampling lattice. The original signal can be perfectly reconstructed if there is no overlapping between these replicas. On the other hand, the sparsest sampling in the spatial domain can be achieved by the tightest arrangement of the spherical replicas in the frequency domain. This can be ensured if the replicas are located around the points of a face-centered cubic (FCC) lattice, which is optimal for sphere packing [CSB87, Slo98, Hal98]. As a consequence, the BCC lattice, which is the reciprocal of the FCC lattice, is optimal for sampling spherically band-limited 3D signals [TMG01].

Although the BCC lattice requires around 30% fewer samples per a unit volume than a CC lattice does for a perfect reconstruction of a spherically band-limited 3D signal [TMG01], it is not widely used for practical applications yet. The reason is mainly the more complicated non-separable resampling scheme, which is required for a BCC-sampled data. For the CC lattice, reconstruction filters are usually designed in 1D, and extended to 2D or 3D by either a separable tensor-product extension [MMK+98] or a spherical extension [ML94]. Although there have been attempts to use separable or radially symmetric filters also for BCC-sampled data [TMG01, TMMG02, Mat03], the results did not live up to the expectations. The separable sheared trilinear interpolation [TMMG02, Mat03] led to a non-isotropic solution, while the spherical filters [TMG01] resulted in blurry images.

The first non-separable box-spline filters, which take the special geometry of the BCC lattice into account, were derived by Entezari et al. [EDM04] demonstrating that the theoretical advantages of BCC sampling can be exploited also in practice. Recently they published a fast evaluation scheme for these filters [EVM08], which turned out to be more efficient than the standard trilinear or tricubic interpolation for CC-sampled data in a software-implemented volume-rendering application. An efficient hardware implementation of box-spline-based resampling, however, has not been published yet.

Csébfalvi recommended a prefiltered reconstruction scheme [Csé05], adapting the concept of *generalized interpolation* [BTU99] to the BCC lattice. According to this approach, first a non-separable discrete prefiltering is performed as a preprocessing, and afterwards a fast separable Gaussian filtering is used for a continuous resampling on the fly. Note that the resulting impulse response is non-separable and not even radially symmetric. This method was extended also to the B-spline family of filters [CH06], and exploiting the separable postfiltering, an efficient hardware implementation was proposed.

In this paper, the B-splines are generalized to the BCC lattice analogously to the Hex-splines. The Hex-splines were proposed by Van de Ville et al. for the hexagonal lattice [VBU04], which is optimal for sampling circularly band-limited 2D signals. The key idea is to take the indicator function of the Voronoi cell corresponding to the BCC lattice as a generating function. The successive convolutions of this generating function with itself yield the family of our BCC-splines. In the following we empirically show that a BCC-spline can be superior over a box spline of the same order of approximation.

2 THE B-SPLINE FAMILY OF FILTERS

In this section we shortly review the B-spline family of filters, as we will generalize them for the the BCC lattice. The B-spline of order zero is defined as a symmetric box filter:

$$\beta^0(t) = \begin{cases} 1 \text{ if } |t| < \frac{1}{2} \\ \frac{1}{2} \text{ if } |t| = \frac{1}{2} \\ 0 \text{ otherwise.} \end{cases} \quad (1)$$

The non-symmetric nearest-neighbor interpolation kernel and $\beta^0(t)$ are almost identical, they differ from each other only at the transition values. Generally, the B-spline filter of order n is derived by successively convolving $\beta^0(t)$ n times with itself. The first-order B-spline is the linear interpolation filter:

$$\beta^1(t) = \beta^0(t) * \beta^0(t) = \begin{cases} 1-|t| \text{ if } |t| \leq 1 \\ 0 \text{ otherwise.} \end{cases} \quad (2)$$

Higher-order B-splines are only approximation filters, as they do not satisfy the interpolation constraint. For example, the cubic B-spline results in a smooth C^2 continuous approximation, therefore it is often used in practice to reconstruct signals that are corrupted by noise. The cubic B-spline is defined as follows:

$$\beta^3(t) = \begin{cases} \frac{1}{2}|t|^3 - |t|^2 + \frac{2}{3} \text{ if } |t| \leq 1 \\ -\frac{1}{6}|t|^3 + |t|^2 - 2|t| + \frac{4}{3} \text{ if } 1 < |t| \leq 2 \\ 0 \text{ otherwise.} \end{cases} \quad (3)$$

Since the Fourier transform of $\beta^0(t)$ is $sinc(\omega/2) = sin(\omega/2)/(\omega/2)$ and the consecutive convolutions in the spatial domain correspond to consecutive multiplications in the frequency domain, the Fourier transform of $\beta^n(t)$ is $sinc^{n+1}(\omega/2)$.

Note that the frequency response of any B-spline takes a value of zero at the centers of all the aliasing spectra (if $\omega = j2\pi$, where $j \in \mathbf{Z} \setminus \{0\}$), therefore a *sample frequency ripple* [ML94] cannot occur. This postaliasing effect arises when the frequency response of the filter is significantly non-zero at the positions representing the "DC" component of the aliasing spectra, and appears in the reconstructed signal as an oscillation at the sample frequency.

The 1D B-splines can be extended to higher-dimensional Cartesian lattices by a tensor product extension. It is easy to see that such an extension of a B-spline of order n provides an approximation order of $n+1$ as the multiplicity of zero at the dual lattice points (except the origin) is at least $n+1$ [SF71].

Figure 1: The Voronoi cell of the BCC lattice.

3 GENERALIZATION FOR THE BCC LATTICE

The separable 3D B-spline of order zero is actually the indicator function of the Voronoi cell corresponding to the Cartesian lattice. Furthermore, the higher-order 3D B-splines can also be obtained by the successive 3D convolutions of this indicator function. This concept can be generalized to the BCC lattice by taking the indicator function of its Voronoi cell (see Figure 1) at the origin as a generating function:

$$\chi_{BCC}(\mathbf{x}) = \begin{cases} 1 \text{ if } \mathbf{x} \in \text{ Voronoi cell,} \\ \frac{1}{m_{\mathbf{x}}} \text{ if } \mathbf{x} \in \text{ boundary of the Voronoi cell,} \\ 0 \text{ if } \mathbf{x} \notin \text{ Voronoi cell,} \end{cases} \quad (4)$$

where $m_{\mathbf{x}}$ is the number of Voronoi cells adjacent at point $\mathbf{x}$. We define the BCC-spline of order zero as $\beta^0_{BCC}(\mathbf{x}) = \chi_{BCC}(\mathbf{x})$. BCC-splines of higher orders are constructed by successive convolutions:

$$\beta^{n+1}_{BCC}(\mathbf{x}) = \frac{(\beta^n_{BCC} * \beta^0_{BCC})(\mathbf{x})}{\Omega}, \quad (5)$$

where Ω is a normalization term defined as the integral of $\chi_{BCC}(\mathbf{x})$:

$$\Omega = \int_{\mathbf{x}\in\mathbf{R}^3} \chi_{BCC}(\mathbf{x})d\mathbf{x}. \quad (6)$$

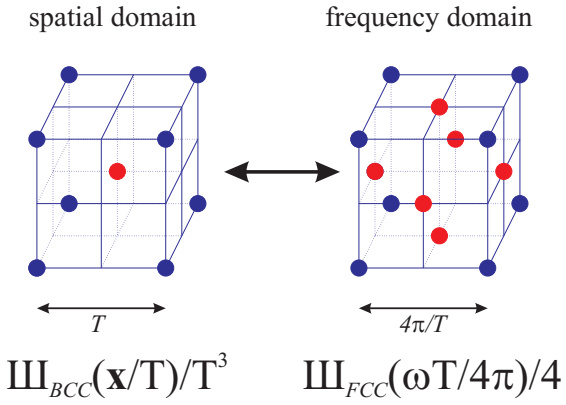

Figure 2: Duality between the FCC and BCC lattices.

4 ORDER OF APPROXIMATION

Note that $\beta^0_{BCC}(\mathbf{x})$ guarantees a *partition of unity* by definition, thus it tiles the 3D space on a BCC pattern:

$$\text{Ш}_{BCC}(\mathbf{x}) * \beta^0_{BCC}(\mathbf{x}) = 1, \quad (7)$$

where $\text{Ш}_{BCC}(\mathbf{x})$ is a *shah* function defined on the BCC lattice (see Figure 2). Transforming Equation 7 into the frequency domain (see the details in the Appendix), we obtain:

$$\frac{1}{4}\text{Ш}_{FCC}\left(\frac{\omega}{4\pi}\right) \cdot \hat{\beta}^0_{BCC}(\omega) = \delta\left(\frac{\omega}{2\pi}\right). \quad (8)$$

According to Equation 8, the Fourier transform $\hat{\beta}^0_{BCC}(\omega)$ of $\beta^0_{BCC}(\mathbf{x})$ takes the value of Ω at the origin and equals to zero at all the other FCC lattice points. Therefore, based on the well-known Strang-Fix conditions [SF71], an approximation order of one is ensured by $\beta^0_{BCC}(\mathbf{x})$. The order of approximation is an asymptotic measure, which expresses how fast the approximate signal $\tilde{f}(\mathbf{x})$ converges to the original signal $f(\mathbf{x})$, when the distance T between the samples is decreased. According to the approximation theory, it depends only on the reconstruction filter $\phi(\mathbf{x})$ that is convolved with the original BCC samples of $f(\mathbf{x})$:

$$f(\mathbf{x}) \approx \tilde{f}(\mathbf{x}) = \frac{\text{Ш}_{BCC}(\mathbf{x}/T) \cdot f(\mathbf{x})}{T^3} * \phi(\mathbf{x}/T). \quad (9)$$

To ensure that $||\tilde{f}(\mathbf{x}) - f(\mathbf{x})||$ tends to zero as T^L, the approximation order of the filter $\phi(\mathbf{x})$ should necessarily be L. When higher-order BCC-splines are constructed, each successive convolution (which is equivalent to a successive multiplication in the frequency domain) increases the multiplicity of zeros (or vanishing moments) by one, thus the approximation order of $\beta^n_{BCC}(\mathbf{x})$ equals to $n+1$.

5 EXPERIMENTAL RESULTS

Non-separable 3D filters have been proposed for the BCC and FCC lattices [EDM04, QEE+05], and recently even for the separable CC lattice [EM06]. Due to their non-separability, however, these filters are either difficult to express by a simple closed form, or computationally expensive to evaluate. Nevertheless, their impulse response can be evaluated in a 3D lookup table in a preprocessing, and afterwards such a discrete approximation can be used for a fast resampling on the fly. Higher-order non-separable filters defined by successive convolutions of a generating function are usually evaluated in the frequency domain [QEE+05, EM06], where the convolution is replaced by a multiplication. We apply the same approach for our BCC-splines of higher orders as well.

Each successive convolution of the generating function increases the support of the resulting BCC-spline filter, but its shape remains the same as that of the Voronoi cell, which is a truncated octahedron (see Figure 1). The slices of the first-order BCC-spline $\beta^1_{BCC}(\mathbf{x})$ are shown in Figure 3. Note that $\beta^0_{BCC}(\mathbf{x})$ and $\beta^1_{BCC}(\mathbf{x})$ are interpolating filters ($\beta^1_{BCC}(\mathbf{x})$ vanishes reaching the first neighboring lattice points), while the higher-order BCC-splines are just approximating filters.

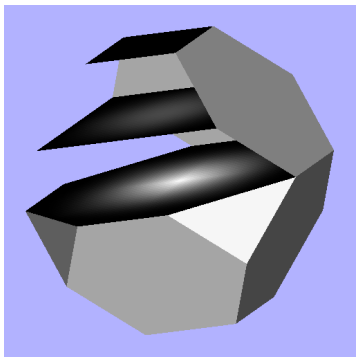

Figure 3: Slices of the first-order BCC-spline.

In order to empirically compare the BCC-splines to the box splines of the same approximation orders, we implemented a software ray caster, which uses a precalculated 3D lookup table of resolution 256^3 for representing the approximate filter kernels. First, we rendered the classical Marschner-Lobb test signal sampled at resolutions of $32\times32\times32\times2$, $64\times64\times64\times2$, and $96\times96\times96\times2$. In Figure 4 the first-order BCC-spline is compared to the linear box spline of the same approximation order. The upper six images show the shaded isosurface of the test signal, whereas the lower six images show the angular error of the gradients calculated by central differencing on the reconstructed function. Although both filters ensure approximately the same speed of convergence, the BCC-spline produces much less annoying artifacts, and it reconstructs the high-

frequency components significantly better, especially when the original signal is not oversampled.

Figure 5 shows the comparison of the third-order BCC-spline to the cubic box spline[1] of the same approximation order. In this case, both filters provide approximately the same image quality and convergence to the original signal. However, the BCC-spline leads to slightly stronger oversmoothing for the lower-resolution representation. For rendering data sets of high signal-to-noise ratio this is clearly a drawback, as the high-frequency details might be removed. On the other hand, practical data sets are usually corrupted by noise, which can be suppressed by a filter of stronger oversmoothing. In order to test the BCC-splines on a real world data set as well, we downsampled an MRI scan of a human brain consisting of $256 \times 256 \times 166$ CC samples onto a lower resolution BCC lattice yielding $128 \times 128 \times 83 \times 2$ BCC samples. Entezari et al. used a similar downsampling [EMBM06] to obtain a BCC representation of an originally CC-sampled data set. However, we exploited that in the frequency domain a perfect low-pass filtering can be performed before the subsampling. Therefore we multiplied the discrete Fourier transform of the original CC-sampled data by the indicator function of the FCC Voronoi cell, that is, the frequency response of the ideal low-pass filter for BCC downsampling. Afterwards we transformed the data back into the spatial domain and took the samples of the BCC sublattice. Figure 6 shows the reconstruction of the human brain from the $128 \times 128 \times 83 \times 2$ BCC samples. The images demonstrate that artifacts caused by the noise and postaliasing are better reduced by the BCC-splines than by the box splines of the same approximation orders.

Concerning the computational cost, the BCC-splines of order one and three require 8 and 64 neighboring voxels to access respectively. It is interesting to note that the equivalent B-splines for the Cartesian lattice require exactly the same number of voxels to read. Nevertheless, using a 3D lookup table to approximate the filter kernels, the BCC-splines are about twice as expensive to evaluate than the box splines of the same approximation orders, since the linear and cubic box splines need just 4 and 32 neighboring voxels to take into account respectively. Thus, the price of the quality improvement is the additional computational cost.

6 CONCLUSION AND FUTURE WORK

In this paper a new family of filters has been proposed for the BCC lattice, which can be interpreted as a non-separable generalization of the separable tensor-product extension of B-splines. It has been empirically demonstrated that, for an additional computational effort, our BCC-splines can provide higher image quality than the box splines of the same approximation orders. For our experiments we approximately evaluated the filter kernels in the frequency domain.

The derivation of the explicit analytical formulas, however, is the subject of our future work. Recently it has been shown that a cubic box spline can be efficiently evaluated by factorizing the filter into a finite difference operator and its Green's function corresponding to the given filter kernel [EVM08]. We plan to follow a similar strategy for the efficient analytical evaluation of our BCC-splines. This would be favorable for a fast hardware implementation as well, since the 3D lookup table representing the approximate filter kernel would not take the texture memory from larger data sets. Furthermore, we would like to derive the frequency responses of these filters in order to quantitatively measure their postaliasing and oversmoothing effect.

An additional possibility for improving the reconstruction of BCC-sampled data is to use a discrete prefiltering before the continuous filtering. For example, the approximation power of higher-order BCC-splines could be better exploited by applying prefitered interpolation or quasi-interpolation schemes.

ACKNOWLEDGEMENTS

This work was supported by the János Bolyai Research Scholarship of the Hungarian Academy of Sciences, OTKA (F68945), the Hungarian National Office for Research and Technology, and Hewlett-Packard. The author of this paper is a grantee of the János Bolyai Scholarship. Special thanks to Alireza Entezari for providing the source code of his linear and cubic box-spline reconstruction routines.

APPENDIX

The *shah* function for the BCC lattice is defined as two overlapping Cartesian *shah* functions:

$$\text{Ш}_{BCC}(\mathbf{x}) = \sum_{i,j,k \in \mathbf{Z}} \delta(\mathbf{x} - [i,j,k]^T) + \sum_{i,j,k \in \mathbf{Z}} \delta\left(\mathbf{x} - \left[i+\frac{1}{2}, j+\frac{1}{2}, k+\frac{1}{2}\right]^T\right). \quad (10)$$

Analogously, the *shah* function for the FCC lattice is constructed as four overlapping Cartesian *shah* functions:

$$\text{Ш}_{FCC}(\mathbf{x}) = \sum_{i,j,k \in \mathbf{Z}} \delta(\mathbf{x} - [i,j,k]^T) + \sum_{i,j,k \in \mathbf{Z}} \delta\left(\mathbf{x} - \left[i, j+\frac{1}{2}, k+\frac{1}{2}\right]^T\right) + \quad (11)$$

[1] In [EDM04] the convolution of the linear box spline with itself is referred to as a "cubic box spline" as it provides the same approximation power as the tricubic B-spline for the CC lattice. Throughout this paper we also use the term "cubic box spline", although this filter is quintic in fact [EVM08], as it consists of quintic polynomials.

$$\sum_{i,j,k\in\mathbf{Z}} \delta\left(\mathbf{x}-\left[i+\frac{1}{2},j,k+\frac{1}{2}\right]^T\right)+$$

$$\sum_{i,j,k\in\mathbf{Z}} \delta\left(\mathbf{x}-\left[i+\frac{1}{2},j+\frac{1}{2},k\right]^T\right).$$

The Fourier transform of III_{BCC} is derived as follows:

$$\mathrm{III}_{BCC}(\mathbf{x}) \Longleftrightarrow \sum_{i,j,k\in\mathbf{Z}} \delta\left(\frac{\omega}{2\pi}-[i,j,k]^T\right)+ \qquad (12)$$

$$\sum_{i,j,k\in\mathbf{Z}} \delta\left(\frac{\omega}{2\pi}-[i,j,k]^T\right)\cdot e^{\mathscr{J}\left[\frac{1}{2},\frac{1}{2},\frac{1}{2}\right]\omega}$$

$$=\sum_{i,j,k\in\mathbf{Z}} \delta\left(\frac{\omega}{2\pi}-[i,j,k]^T\right)\left(1+(-1)^{(i+j+k)}\right)$$

In Equation 12 only those terms are non-zero, where $i+j+k$ is even. This is possible if all these three integers are even, or two of them are odd and one is even. Thus we can separate the sum into four terms:

$$\mathrm{III}_{BCC}(\mathbf{x}) \Longleftrightarrow \sum_{l,m,n\in\mathbf{Z}} \delta\left(\frac{\omega}{2\pi}-[2l,2m,2n]^T\right)\cdot 2+ \qquad (13)$$

$$\sum_{l,m,n\in\mathbf{Z}} \delta\left(\frac{\omega}{2\pi}-[2l,2m+1,2n+1]^T\right)\cdot 2+$$

$$\sum_{l,m,n\in\mathbf{Z}} \delta\left(\frac{\omega}{2\pi}-[2l+1,2m,2n+1]^T\right)\cdot 2+$$

$$\sum_{l,m,n\in\mathbf{Z}} \delta\left(\frac{\omega}{2\pi}-[2l+1,2m+1,2n]^T\right)\cdot 2$$

Exploiting that $\delta(A\omega)=\delta(\omega)/det(A)$, we obtain:

$$\mathrm{III}_{BCC}(\mathbf{x}) \Longleftrightarrow \sum_{l,m,n\in\mathbf{Z}} \delta\left(\frac{\omega}{4\pi}-[l,m,n]^T\right)\cdot\frac{1}{4}+ \qquad (14)$$

$$\sum_{l,m,n\in\mathbf{Z}} \delta\left(\frac{\omega}{4\pi}-\left[l,m+\frac{1}{2},n+\frac{1}{2}\right]^T\right)\cdot\frac{1}{4}+$$

$$\sum_{l,m,n\in\mathbf{Z}} \delta\left(\frac{\omega}{4\pi}-\left[l+\frac{1}{2},m,n+\frac{1}{2}\right]^T\right)\cdot\frac{1}{4}+$$

$$\sum_{l,m,n\in\mathbf{Z}} \delta\left(\frac{\omega}{4\pi}-\left[l+\frac{1}{2},m+\frac{1}{2},n\right]^T\right)\cdot\frac{1}{4}$$

$$=\frac{1}{4}\mathrm{III}_{FCC}\left(\frac{\omega}{4\pi}\right).$$

REFERENCES

[BTU99] T. Blu, P. Thévenaz, and M. Unser. Generalized interpolation: Higher quality at no additional cost. In *Proceedings of IEEE International Conference on Image Processing*, pages 667–671, 1999.

[CH06] B. Csébfalvi and M. Hadwiger. Prefiltered B-spline reconstruction for hardware-accelerated rendering of optimally sampled volumetric data. In *Proceedings of Vision, Modeling, and Visualization*, pages 325–332, 2006.

[CSB87] J. H. Conway, N. J. A. Sloane, and E. Bannai. *Sphere-packings, lattices, and groups*. Springer-Verlag New York, Inc., 1987.

[Csé05] B. Csébfalvi. Prefiltered Gaussian reconstruction for high-quality rendering of volumetric data sampled on a body-centered cubic grid. In *Proceedings of IEEE Visualization*, pages 311–318, 2005.

[EDM04] A. Entezari, R. Dyer, and T. Möller. Linear and cubic box splines for the body centered cubic lattice. In *Proceedings of IEEE Visualization*, pages 11–18, 2004.

[EM06] A. Entezari and T. Möller. Extensions of the Zwart-Powell box spline for volumetric data reconstruction on the Cartesian lattice. *IEEE Transactions on Visualization and Computer Graphics (Proceedings of IEEE Visualization)*, 12(5):1337–1344, 2006.

[EMBM06] A. Entezari, T. Meng, S. Bergner, and T. Möller. A granular three dimensional multiresolution transform. In *Proceedings of Joint EUROGRAPHICS-IEEE VGTC Symposium on Visualization*, pages 267–274, 2006.

[EVM08] A. Entezari, D. Van De Ville, and T. Möller. Practical box splines for reconstruction on the body centered cubic lattice. *to appear in IEEE Transactions on Visualization and Computer Graphics*, 2008.

[Hal98] T. C. Hales. Cannonballs and honeycombs. *AMS*, 47(4):440–449, 1998.

[Mat03] O. Mattausch. Practical reconstruction schemes and hardware-accelerated direct volume rendering on body-centered cubic grids. *Master's Thesis, Vienna University of Technology*, 2003.

[ML94] S. Marschner and R. Lobb. An evaluation of reconstruction filters for volume rendering. In *Proceedings of IEEE Visualization*, pages 100–107, 1994.

[MMK+98] T. Möller, K. Mueller, Y. Kurzion, R. Machiraju, and R. Yagel. Design of accurate and smooth filters for function and derivative reconstruction. In *Proceedings of IEEE Symposium on Volume Visualization*, pages 143–151, 1998.

[OS89] A. V. Oppenheim and R. W. Schafer. *Discrete-Time Signal Processing*. Prentice Hall Inc., Englewood Cliffs, 2nd edition, 1989.

[QEE+05] W. Quiao, D. S. Ebert, A. Entezari, M. Korkusinski, and G. Klimeck. VolQD: Direct volume rendering of multi-million atom quantum dot simulations. In *Proceedings of IEEE Visualization*, pages 319–326, 2005.

[SF71] G. Strang and G. Fix. A Fourier analysis of the finite element variational method. In *Constructive Aspects of Functional Analysis*, pages 796–830, 1971.

[Slo98] N. J. A. Sloane. The sphere packing problem. In *Proceedings of International Congress of Mathematicians*, pages 387–396, 1998.

[TMG01] T. Theußl, T. Möller, and M. E. Gröller. Optimal regular volume sampling. In *Proceedings of IEEE Visualization*, pages 91–98, 2001.

[TMMG02] T. Theußl, O. Mattausch, T. Möller, and M. E. Gröller. Reconstruction schemes for high quality raycasting of the body-centered cubic grid. *TR-186-2-02-11, Institute of Computer Graphics and Algorithms, Vienna University of Technology*, 2002.

[VBU04] D. Van De Ville, T. Blu, and M. Unser. Hex-splines: A novel spline family for hexagonal lattices. *IEEE Transactions on Image Processing*, 13(6):758–772, 2004.

$32 \times 32 \times 32 \times 2$ voxels. $64 \times 64 \times 64 \times 2$ voxels. $96 \times 96 \times 96 \times 2$ voxels.

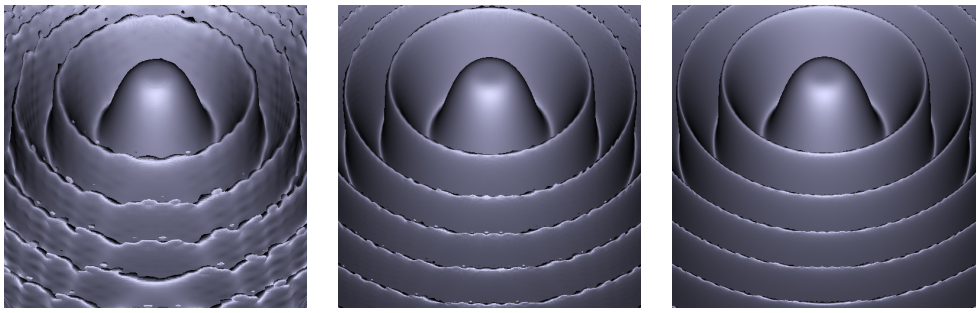

Isosurface reconstruction using the first-order BCC-spline.

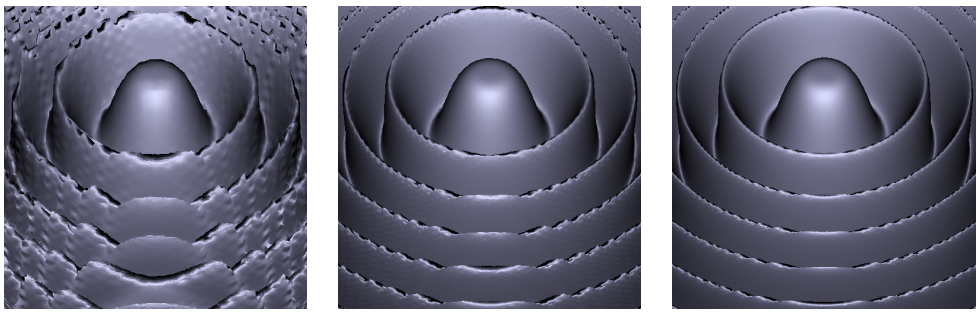

Isosurface reconstruction using the linear box spline.

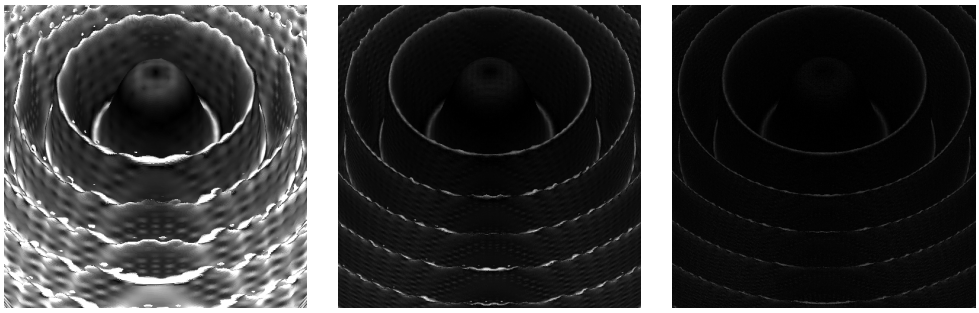

Angular error of the gradients calculated with the first-order BCC-spline.

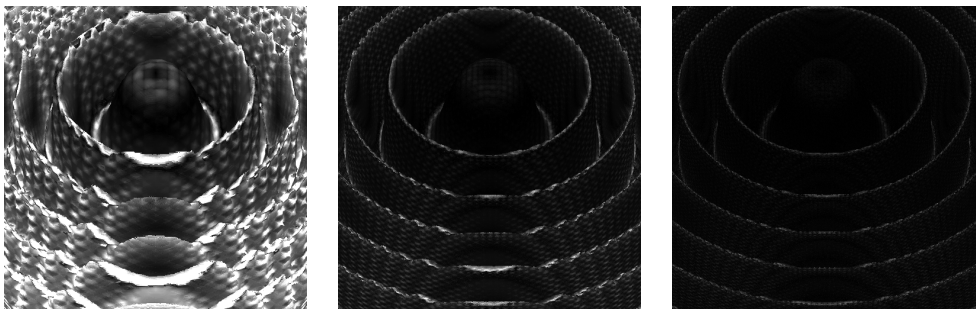

Angular error of the gradients calculated with the linear box spline.

Figure 4: Reconstruction of the Marschner-Lobb signal using the first-order BCC-spline and the linear box spline of the same order of approximation. In the error images the angular error of zero degree is mapped to black, whereas the angular error of 30 degrees is mapped to white.

$32 \times 32 \times 32 \times 2$ voxels. $64 \times 64 \times 64 \times 2$ voxels. $96 \times 96 \times 96 \times 2$ voxels.

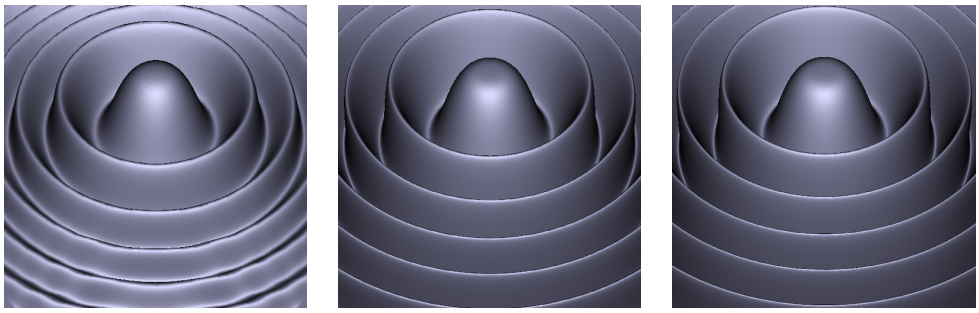

Isosurface reconstruction using the third-order BCC-spline.

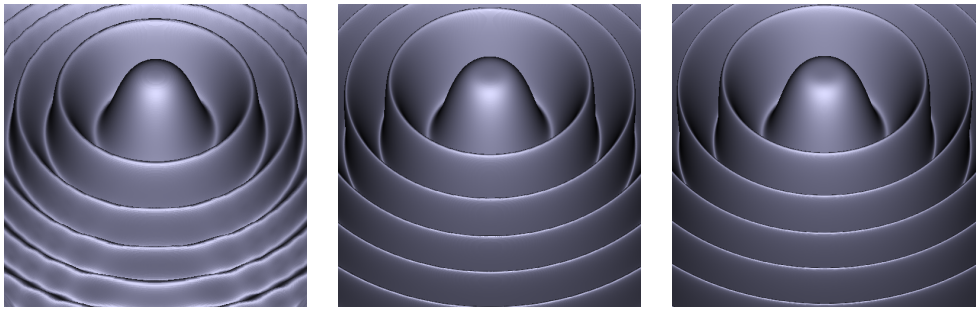

Isosurface reconstruction using the cubic box spline.

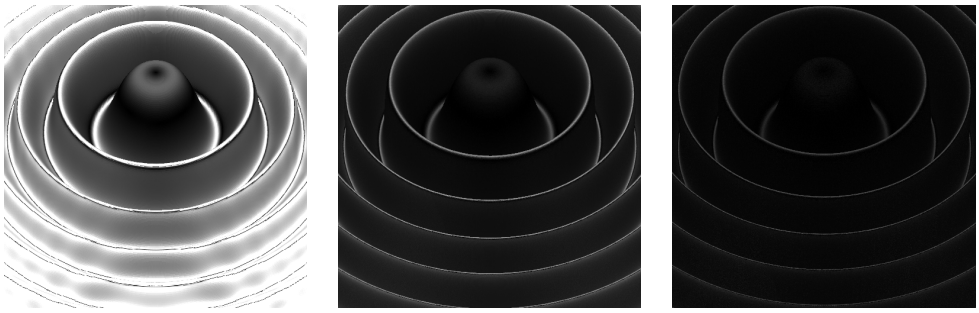

Angular error of the gradients calculated with the third-order BCC-spline.

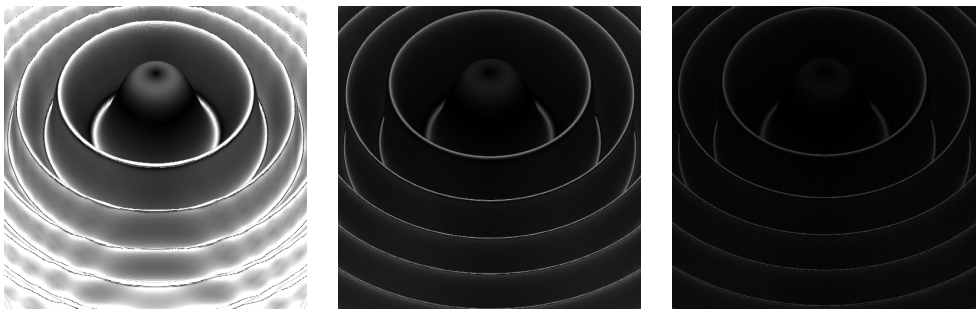

Angular error of the gradients calculated with the cubic box spline.

Figure 5: Reconstruction of the Marschner-Lobb signal using the third-order BCC-spline and the cubic box spline of the same order of approximation. In the error images the angular error of zero degree is mapped to black, whereas the angular error of 30 degrees is mapped to white.

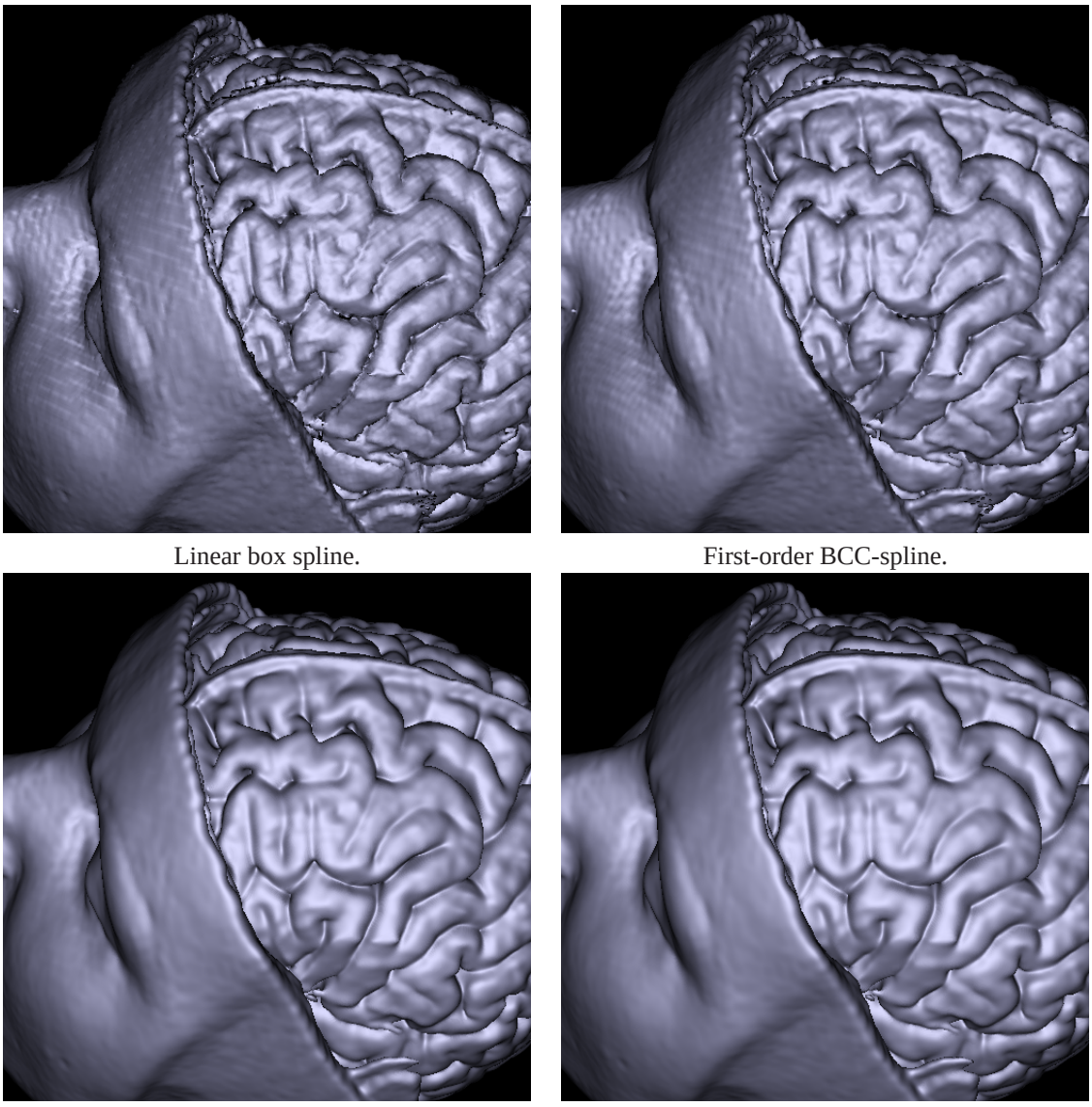

Linear box spline. First-order BCC-spline.

Cubic box spline. Third-order BCC-spline.

Figure 6: Reconstruction of a human brain from $128 \times 128 \times 83 \times 2$ BCC samples of an MRI scan.